BOLLETTINO DI GEOFISICA TEORICA ED APPLICATA VOL. XXXVI, N. 141-144 - MARCH-DECEMBER 1994

G. GASPAROTTO [1] and C. SAVELLI [2]

MINERAL CHEMISTRY OF THE CALCALKALINE LAVAS FROM MARSILI SEAMOUNT (SOUTHEAST TYRRHENIAN SEA): SOME MAGMATOLOGICAL AND GEODYNAMIC CONSIDERATIONS

Abstract. Mineral chemistry data from lavas recovered over a large depth interval of the deep-water volcano of Marsili (Aeolian back-arc, SE Tyrrhenian Sea) are presented. The volcano is built up by products of calcalkaline affinity (20 samples) with the only exception of one outcrop of sub- alkaline, within-plate basalts in the crestal area. Petrography and mineral chemistry data indicate that the low parts of edifice consist of basalts which present a porphyritic vesicular texture. Basalt phenocryst assemblages consist either of plagioclase and little olivine and clinopyroxene (porphyritic index, P.I. about 13%) or of olivine and scarce pyroxene and plagioclase (P.I. < 5%). The summit area is constructed by andesites which have a porphyritic texture (P.I. about 15%) with plagioclase and little clino- and ortho-pyroxene and magnetite. On the whole, the calcalkaline lavas of Marsili have bimodal composition, and consist of basalts and andesites with, respectively, calcalkaline and high-K serial affinity. The andesites mark a change in the geodynamic conditions that is reflected by the clockwise rotation of the seamount rifting from the early NNE-SSW orientation, associated with the extrusion of the basalts, to a dominant tensional regime trending almost NE-SW. This evolution is discussed in the context of some magmatic- structural features in the south-east Tyrrhenian volcanic area. The region is characterized by continental arc volcanism migration from the island of Sardinia, to the central Tyrrhenian Sea, to the Aeolian area.

INTRODUCTION

Marsili volcano is a prominent physiographic feature emplaced (Fig. 1 and inset) in the Marsili basin, one of the youngest existing deepwater basins. The inception of volcanic activity in the SE Tyrrhenian Sea occurred in a well-constrained time interval ranging from 1.9 to 1.7 Ma ago (Site 650 of the Ocean Drilling Program) (Kastens et al., 1986; 1988). This magmatism (Fig. 1) of andesitic-basaltic composition produced the western margin of the deep-seated igneous crust that surrounds the Marsili seamount (Beccaluva et al., 1990). Similarly to the great volcanoes Magnaghi and Vavilov, the seamount under study developed on oceanic basement. The deep basin surrounding Marsili volcano is bounded to the south and east by the tightly concave volcanic arc of the Aeolian islands and adjoining seamounts (e.g., Barberi et al., 1974; Beccaluva et al., 1985; Francalanci et al., 1989; Crisci et al., 1991: Francalanci and Manetti, this vol.). All these volcanic structures rest above a Wadati-Benioff zone. Fig. 2 shows the distribution of the deep, subcrustal foci of the Tyrrhenian seismogenic zone (Ritsema, 1979; Gasparini et al., 1982; Anderson and Jackson, 1987; Giardini and Velonà, 1991).

Maccarrone (1970) and Keller and Leiber (1974) studied the petrochemical characteristics of Marsili lavas and tried a comparison with the products from the adjoining volcanic areas, in particular the Aeolian arc. Selli et al. (1977) provided new lava analyses and datings of less than 0.2 Ma and discussed some significant tectonic features of the seamount under study.

Manuscript received, December 30, 1992; accepted September 15, 1993.

[1] Dipartimento di Scienze Mineralogiche, Università, Piazza di Porta S. Donato 1, 40126 Bologna, Italy.

[2] Istituto per la Geologia Marina, Via Gobetti 101, 40129 Bologna, Italy.

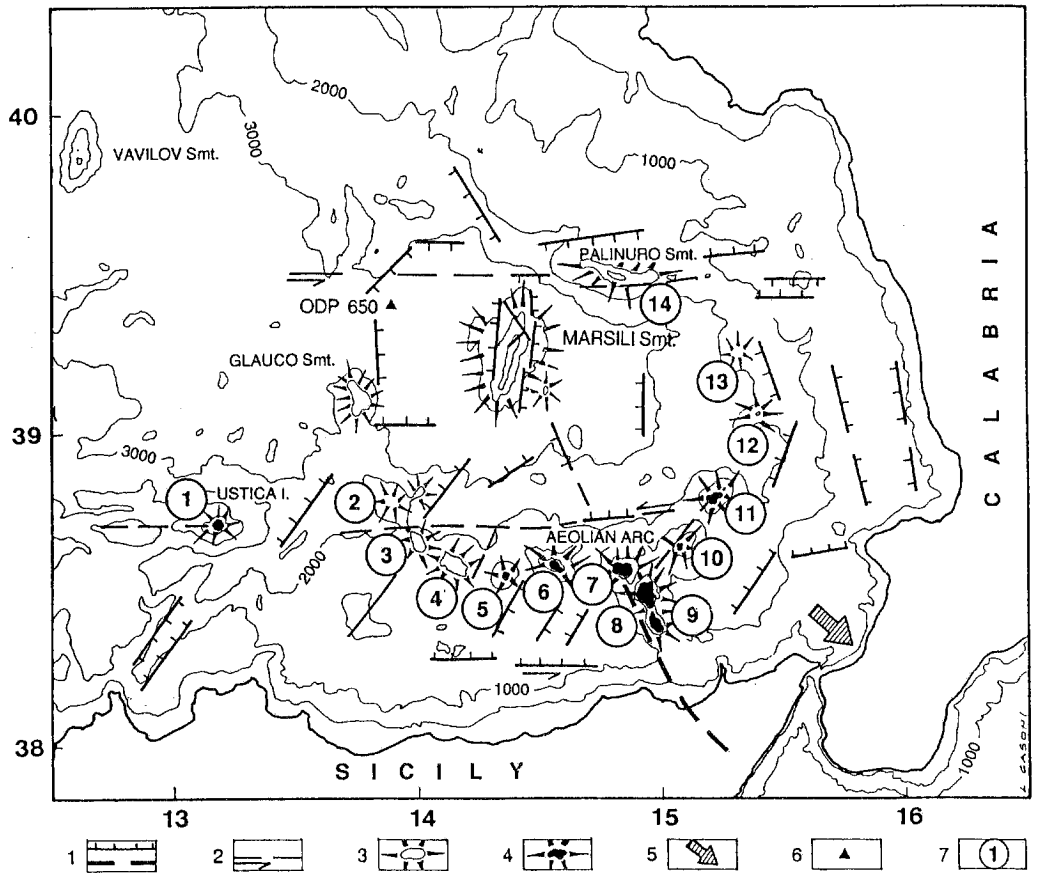

Fig. 1 — Bathymetric and tectonic sketch map of the Southeastern Tyrrhenian volcanic region (Aeolian arc and deep basin of Marsili), modified after Boccaletti et alii (1984 and 1990) and Doglioni (1991). 1, major normal faults; 2, major strike-slip faults (small arrows indicate the sense of motion); 3, submerged and 4, outcropping volcanic centers (v. islands); 5, present-day slip vector of the Calabrian arc; 6, drill-site 650 of the Ocean Drilling Program; 7 (circled numbers), main volcanic centers: (1), Isl. of Ustica; (2), Sisifo smt.; (3), Enarete smt.; (4), Eolo smt.; (5), Isl. of Alicudi; (6), Isl. of Filicudi; (7), Isl. of Salina; (8), Isl. of Lipari; (9), Isl. of Vulcano; (10), Isl. of Panarea; (11), Isl. of Stromboli; (12), Lametini smt.; (13), Alcione smt.; (14), Palinuro smt. The region of the deep basin of Marsili is bounded by the important E-W trending shear zones of the Palinuro located to the north and of the Sicily continental slope to the south. The strike-slip movements are compensated by the development of prevailing clockwise fault-block rotations and tectonic structures oriented NE-SW (Boccaletti et al., 1984; Finetti and Del Ben, 1986).

With regard to the tectonism, notable movements of distension and subsidence affected the Marsili basement (Finetti and Del Ben, 1986; Kastens et al., 1988; Mascle and Rehault, 1990; Wang et al., 1991). The occurrence of tectonic distension on the seamount itself was documented by the investigations of the R/Vessels Vityaz (1986) and Akademic Mstislav Keldysh (1988) of the USSR Academy of Sciences (Sborshchikov et al., 1988 and 1990; Savelli, 1993.).

Information about the mineralogical composition of Marsili volcanics may contribute to a better understanding of the nature of basic igneous crust of back-arc setting emplaced at the edge of an orogene. Morever, the oceanic crust around the seamount likely precludes assimilation of continental crust, similar to that recognized in Aeolian arc volcanoes (e.g., Bargossi et al., 1990; Peccerillo and Wu, 1992).

This work aims at defining the mineralogy of lavas from Marsili deep-water seamount and at discussing the magmatic evolution and tectonic context. In particular, the mineral chemistry data were obtained on nine selected lava samples recovered during the two cruises of the Russian

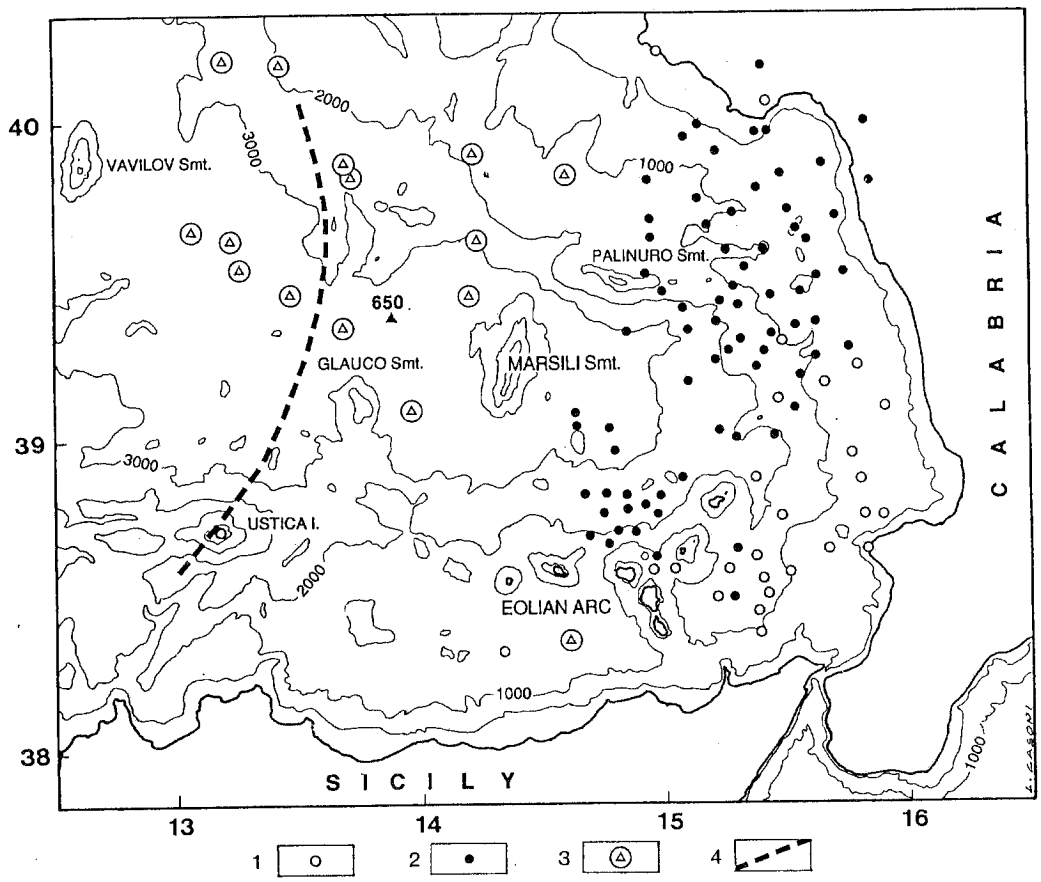

Fig. 2 — Distribution of the deep foci in the southern Tyrrhenian seismogenic volcanic area fter Giardini and Velona' (1991). Depth of foci: 1 = 100-250 km; 2 = 250-350 km; 3 = > 350 km; 4 = main deep-seated structural discontinuity (from Anchise seamount-Ustica Island to Issel seamount) roughly corresponding to the loci of the relict volcanic arc of the Pliocene (4-2 Ma?) between the Marsili and Vavilov basins. Triangle = drill-site 650 of the Ocean Drilling Program.

ships mentioned above. A more comprehensive account of the geochemistry of Marsili volcanites is given elsewhere (Savelli and Gasparotto, 1994).

TECTONIC SETTING

The main part of the volcano under study is characterized by the presence of linear tensional faults trending N-S to NNE-SSW (Selli et al., 1977; Finetti and Del Ben, 1986; Sborshchikov et al., 1988 and 1990; Savelli, 1993). However, the summit exhibits fractures and open fissures which are NE-SW oriented as a consequence of clockwise rotation of the rifting. The extension associated with the spreading mechanisms of the top area is in the NW-SE direction, while, during the early to intermediate periods of volcanic activity in the lower part of the edifice, it was directed E-W to WNW-ESE.

The igneous basement surrounding the Marsili seamount was affected by notable subsidence (not less than about 700 m/Ma; Wang et al., 1991). The Marsili area and Aeolian volcanoes are floored with different types of crust. Indeed, the Aeolian arc is resting on crust of transitional type which is 15-20 km thick (Morelli et al., 1975; Nicolich, 1981; Boccaletti et al., 1990) as compared to the 6 km thickness of the oceanic crust of Marsili basin.

Table 1 — Location of sampling stations and scheme of main petrographic feature of samples from Marsili seamount.

CA = calcalkaline; HK = high potassium calcalkaline; WP = intra-plate (i.e. ocean island basalt, OIB); OL = olivine; PL = plagioclase; CPX = clinopyroxene; OPX = orthopyroxene; GL = glass; SP = spinel; ZE = zeolite; CC = calcite; AMP = amphibole; MT = magnetite; AP = apatite; OP = opaques; ( ) = minerals present in small amount; mp. = microphenocrysts; v. = vesicular; vv. = very vesicular; p. = porphyritic; f. = fragments; a. = aphyric; fl. = fluidal texture; b. sfl. = below seafloor.

Station	LAT. N	LONG. E	Depht (m)	Rock Type	Phenocrysts	Groundmass	Notes
MIR 1-4	39°19.6'	14°24.9'	1500	CA-Basalt	OL-PL	PL-OL-GL-CPX	v.p.
MIR 1-3	39°20.0'	14°26.4'	2010	CA-Basalt	PL-CPX-OL	PL-CPX-OL	vv.
VI-1663 core	39°24.2'	14°20.5'	3080	CA-Basalt	PL-OL	PL-CPX-OL-GL	v. f. (155-164 cm b. sfl)
M22-103 core	39°04.5'	14°23.2'	3200	CA-Basalt	OL-CPX	GL-PL-SP	v. f. corer bottom
MIR 1-1	39°20.3'	14°27.2'	2590	CA-Basalt	OL-PL	PL-CPX-OL-GL	v. p.
MIR 1-2	39°20.2'	14°26.9'	2450	CA-Basalt	OL-PL	PL-OL-CPX-GL	vv.
VI-1661 core	39°17.95'	14°24.0'	920	CA-Basalt	PL-CPX-OL	PL-CPX-GL	v. f. (30-0 cm b. sfl.)
MAC-4D from	39°14.09'	14°22.05'	677	CA-Basalt	mp. PL-CPX-OL	PL-CPX-OP-GL-ZE-CC	a. v.
to	39°14.09'	14°22.05'	677				
T72-14 from	39°08.1'	14°21.5'	1350	CA-Bas-And.	PL-CPX-OL	PL-PX-GL	
to	39°08.4'	14°19.7'	1000				
VI-1691 from	39°12.1'	14°21.1'	1100	HK-Bas-And.	PL-CPX-OL (OPX)	PL-CPXGL-SP (OPX)	v.
to	39°12.3'	14°22.3'	760				
MAC-4B from	39°14.09'	14°22.05'	677	HK-Bas-And.	mp. PL-CPX-OL	GL-OP-ZE-CC	
to	39°14.09'	14°22.05'	677				
T72-17 from	39°06.3'	14°17.3'	2606	CA-Andesite	PL-CPX-OPX-(AMP)	PL-PX-GL-AMP	
to	39°07.7'	14°17.3'	2300		OL	MT	
VI-1657 from	39°17.0'	14°22.8'	1170	HK-Andesite	PL-CPX-OPX-MT	PL-CPX-MT-GL	
to	39°16.9'	14°23.6'	1270				
M22-104 core	39°04.8'	14°23.2'	3300	HK-Andesite	CPX-PL-OL-(SP)	GL-PL	v. f. corer bottom
MIR 2-1	39°17.2'	14°23.5'	505	HK-Andesite	PL-CPX-OPX-MT	PL-CPX-MT-GL	v. fl.
VI-1656 from	39°17.0'	14°23.1'	1000	HK-Andesite	PL-CPX-OPX-MT	PL-CPX-MT-GL	
to	39°17.0'	14°24.1'	700				
MAC-3 from	39°16.09'	14°24	750	HK-Andesite	PL-CPX-OPX-AMP	GL-PL-CPX-OP-AP	p. v.
to	39°17.06'	14°24	772				
MIR 2-3	39°17.2'	14°23.5'	503	HK-Andesite	PL-CPX-OPX-MT	PL-CPX-MT-GL	p. v. fl.
CST-68-13 core	39°17.2'	14°24.3'	651	HK-Andesite	PL-CPX-OPX-(AMP)	GL-PL-PX-OP	v.
CT-69-30 from	39°16.9'	14°23.5'	628	HK-Andesite	PL-CPX-OPX-(AMP)	GL-PL-PX-OP	v.
to	39°17.0'	14°23.9'	618		(OL)		
CT69/27/2A from	39°14.2'	14°22.6'	771	WP-basalt	PL-OL-(CPX)-GL	GL-OP-PL-PX	
to	39°14.1'	14°22.0'	760			MT-AP	

Two great east-west trending strike-slip zones (Fig. 1) are located to the north and south of the Marsili deep basin (Boccaletti et al., 1984, 1990; Finetti and Del Ben, 1986; Lavecchia, 1988; Savelli and Schreider, 1991; Locardi and Nicolich, 1992). They are known, respectively, as the **Palinuro volcano** and the **Sicilian slope** lineation zones. Along the northern alignment is the E-W trending volcanic seamount of Palinuro. Along the southern wide, tectonic lineation zone, affected by complex strike-slip displacements, are located several volcanic edifices of the Aeolian arc. The left-lateral motions of the magmato-tectonic lineation zones are associated with development of prevailingly clockwise fault-block rotations (Doglioni, 1991). Another major regional (Fig. 1), tectono-magmatic structure is the alignment Lipari-Taormina (Neri et al., 1991). Along this fracture system, which interrupts the north Sicilian slope E-W trending lineation zone, are located the central Aeolian volcanic islands of Salina, Lipari and Vulcano, separating the western sector (Beccaluva et al., 1985) of the archipelago from the eastern one.

The Marsili, its adjacent deep-seated igneous crust and the Aeolian volcanoes have developed in a tectonic setting of west dipping subduction (Scandone, 1980; Kastens et al., 1990; Mascle et al., 1990; Doglioni, 1991, 1992; Gasperini 1993). From the geodynamic point of view, the spreading in the southern Tyrrhenian is compensated by drift (Savelli, 1988; Sartori, 1990) of the neighbouring oroclines of Calabria and Sicily.

The Marsili deep basin and adjoining Aeolian arc are emplaced above the Tyrrhenian seismogenic zone (Fig. 2; Ritsema, 1979; Gasparini et al., 1982; Anderson and Jackson, 1987; Giardini and Velona', 1991). Fig. 2 shows the distribution of foci deeper than 100 km; the Benioff zone length is small, about 120 km, with respect to its maximum focal depth, about 500 km. The geometry (Barberi et al., 1974; Anderson and Jackson, 1987; Giardini and Velona', 1991) is, on the whole, anomalous compared with a standard geometry of slab subduction where a parallelism between volcanic arc and deep foci exists. The dip of the Benioff zone changes at the depth of about 250 km, its angle of 70° becoming less vertical (45 -50°) at greater depth.

PHYSIOGRAPHY

Marsili seamount is a large volcano, about 55 km long and 25 wide (Fig. 3; Selli et al., 1977; Puchelt and Laschek, 1986), emplaced in the central sector of a deepwater basin. Fig. 1 shows that the basin, a subcircular, elliptical physiographic feature reaching a water depth of 3400 - 3500 m, is somewhat elongated in the east-south-east direction, and covers an area surface of about 8000 km^2 including the central axial seamount.

The seamount is almost 3 km high, excluding its lowermost portions which are covered by sediments. The summit reaches the depth of 485 m below sea level (Sborshchikov et al., 1988); the base lies at depths between 3400 to somewhat less than 3100 m on the northern edge. This edge is close to the lower continental slope area that surrounds the Marsili deepwater basin off the coasts of Calabria and Sicily. The overall elongations of the volcano and its two lateral ridges are the same, all striking approximately N10-20°E. The crestal zone of the seamount is approximately 20 km long above the 1000 m depth contour, and contains several elevations. Three clearly different summit areas situated in the southern, central and northern segment of the shallow axial zone can be recognized from the bathymetric surveys. Overall, the size of crestal structures increases from south to north.

The meridional summit area is the smallest. Its top lies at 739 m below sea level and its length is approximately 2.5 km. The structure is N10-20°E trending parallel to the overall lineation of the seamount. The central summit area, separated from the former by a saddle enclosed within the 950 bathymetric line, is the longest (approximately 10 km), and is almost north-south trending (N5°E) in its central segment. This segment is topped by two elongated elevations. They culminate at depths of 650 and 639 m, respectively.

The third, northern crestal zone, separated from the adjoining one to the south by the 800 m depth contour, contains the Marsili summit (485 m b.s.l.). Its overall orientation (Selli et al., 1977; Sborshchikov et al., 1990) is NE-SW, clearly oblique with respect to the elongation of the central and southern crestal parts.

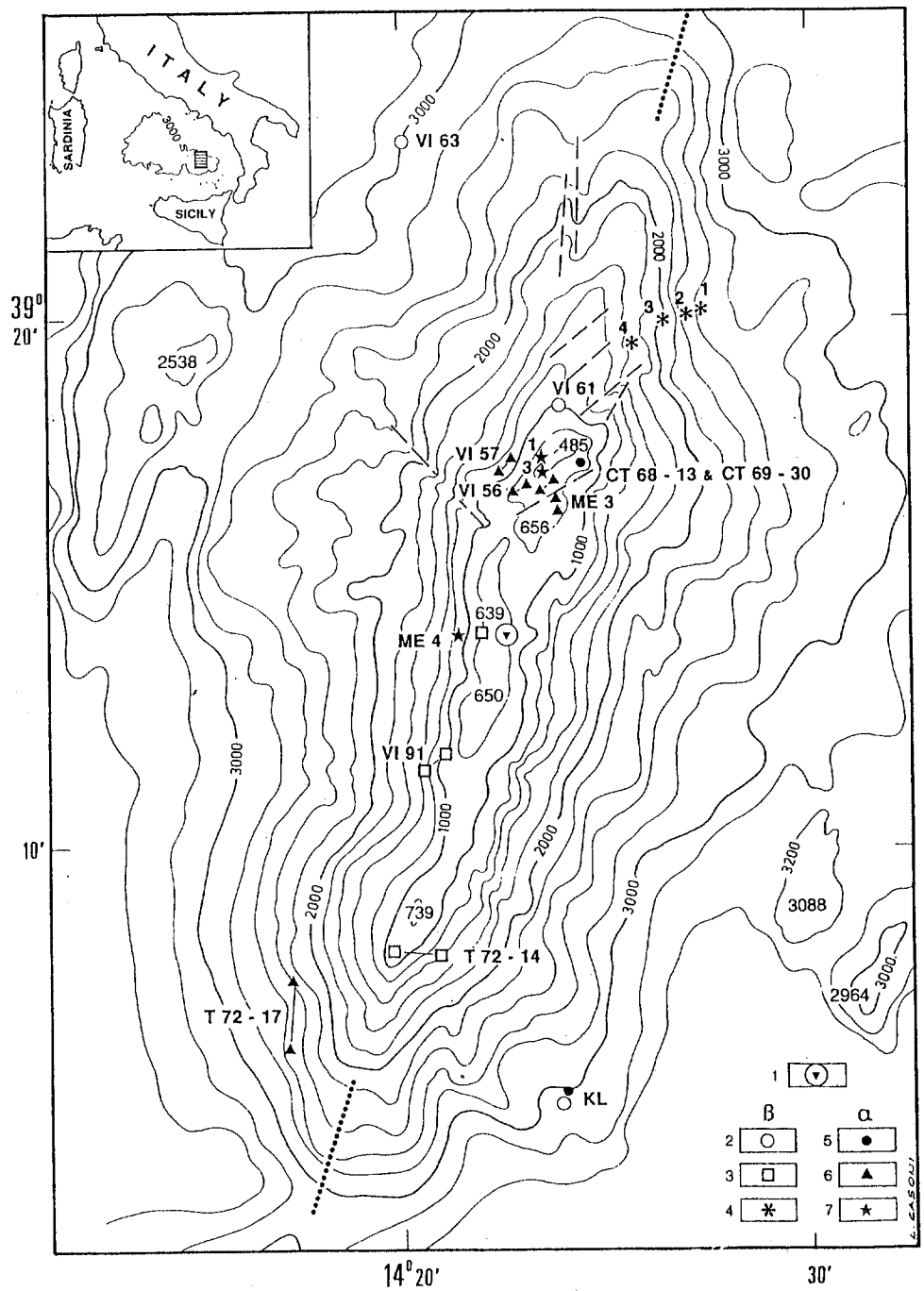

Fig. 3 — Morphology of the Marsili volcanic seamount; bathymetry according to map N. 1602 of the Istituto Idrografico della Marina. Location of sampling sites. 1 = dredge site of basalts with OIB serial affinity (Station CT69/27 of Selli et al., 1977). Lavas of calcalkaline serial affinity (beta= basalts, alpha= andesites), 2= coring sites of basalts and andesitic basalt; 3= dredge sites of basalts and andesitic basalt; 4= sampling sites of basalts recovered during dive n. 21 of MIR-1 submersible; 5 = coring sites of andesites; 6= dredge sites of andesites; 7= submersible MIR-2 dive n. 16, sampling sites of HK-CA andesites (near the top). Dashed lines=fractures in the northern area from Selli et alii (1977), modified according to Puchelt and Laschek (1986) and Sborshchikov et alii (1990).

Table 2 — Point count modal analyses of selected samples.

	M1-2	M1-3	And
Pl	0.3	16.9	10.1
Ol	4.7	(+)	(+/—)
Cpx	(+)	2.8	1.3
Opx	(—)	(—)	0.5
Mt	(—)	(—)	0.6
Gms	95.0	80.3	87.5

(+)=scarce; (—)=absent; (+/—)=accidental; M1-2, M1-3: basalts; And=mean of 3 andesites.

The main axial structure of Marsili (Fig. 3) is flanked by two physiographic highs located 15 km from the axis, to the northwest and southeast. Fig. 3 shows that the lateral lava crests of the volcano are separated by different depth contours from the main edifice (respectively, 3000 and 3200 m) and that they have different sizes, that located to the northwest being larger and shallower. The northwestern foothill is 17 km long and lies between 3400 and 2538 m of depth. On the other side, the lateral ridge to the southeast is 7 km long and its elevation varies from 3350 to 2964 m. This physiographic feature is more distant from the Marsili axis compared with its counterpart to the northwest. Another elongated high of about 260 m (3350 to 3088 m) covering an area surface somewhat smaller is situated between the high mentioned above and the lower rim of the central edifice.

The main bulk of the Marsili volcano is, probably, Late Quaternary in age. The existence of young eruptive activity on the summit area is indicated by K/Ar dating of less than 0.2 Ma (Selli et al., 1977), and by Mir dive observations and deep-tow TV and photo images which show fresh lava surfaces and lack of sediments. The positive magnetic anomaly of high intensity, which is closely associated with the edifice suggests an age not older than the beginning of the Brunhes polarity epoch (0.7 Ma) for the volcanites of the seamount (Savelli and Schreider, 1991).

The two small structures bordering the Marsili are probably older than the Brunhes because of their association with negative magnetic anomalies.

In situ observations from the Mir submersibles shed light on some characteristics of the lava eruptions and the magmato-tectonic history of the seamount (Sborshchikov et al., 1988, 1990; Savelli, 1993). The pillows are often elongated in shape, and in some places form very steep, almost vertical "cascades" of lava tubes. Linear fault scarps, pillow ridges and open fissures (gjar) occur parallel to the main axial elongation of the seamount; these tectonic features indicate the presence of active rifting processes. Moreover, it was recognized (Sborshchikov et al., 1988; Savelli, 1993) that the eruptive products of the summit consist of scoriaceous flows, whereas pillow lavas form the deep portions of the seamount at water depths greater than 1000-1100 m. This morphologic change of the lavas seems to be accompanied by a change of the fault lineations that trend NNE-SSW in the deep- intermediate parts, whereas they have an anti-Apenninic direction (NE-SW) in the summit area of Marsili.

VOLCANITES

Methods of analyses

Mineral analyses were performed at the "Dipartimento di Scienze Mineralogiche - Bologna University" with a Philips 515 SEM, equipped with an EDS spectrometer. Operating conditions were 15 kV accelerating voltage, 2 nA sample current, and 100 live seconds counting time. A wide range of natural mineral standards (kindly supplied by the USMN, Washington D. C.; Jarosewich et al., 1986) was used to minimize matrix effects.

Major and trace elements were analyzed at the "Service d'Analyses des Roches et Mineraoux du CNRS, CRPG, Vandoeuvre-les-Nancy, France" with plasma spectrometry (Govindaraju and Mevelle, 1987).

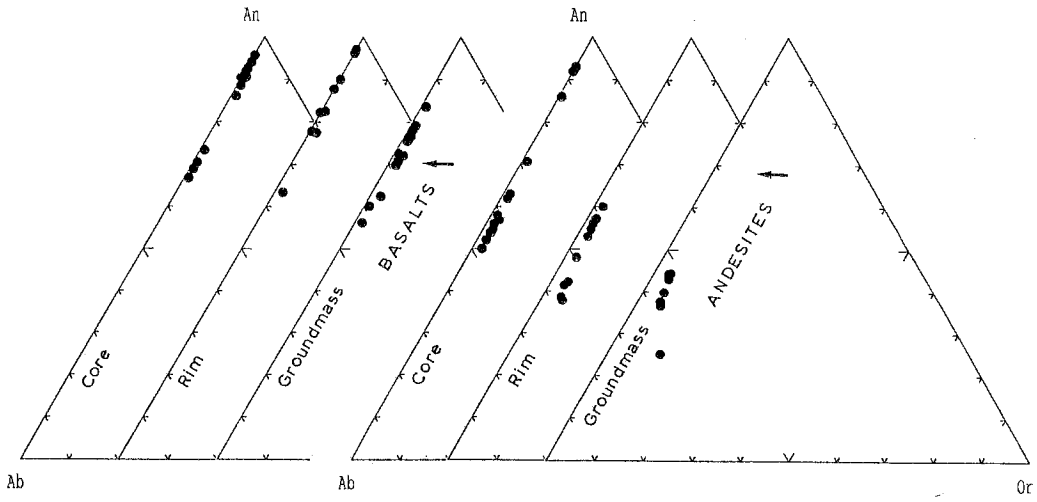

Fig. 4 — Ternary diagram Albite-Anorthite-Orthoclase (Ab-An-Or) of plagioclases in lavas from Marsili volcano.

Petrography

The new samples recovered form the Marsili Seamount are 6 basalts, 6 andesites and 1 basaltic andesite. Sampling sites are listed in Table 1 and shown in Fig. 3, while in Table 2 are reported point counted modal analyses of selected samples. The rocks are characterized by a notable freshness.

The basalts are texturally heterogeneous: some samples are characterized by porphyritic-vesicular textures with low P.I. (<5%; e.g. sample M1-2 of Table 2); phenocrysts are represented by little olivine with minor clinopyroxene and scarce plagioclase. Other samples have a higher P.I. (about 20%; sample M1-3 of Table 2) with plagioclase as the most abundant phenocryst, and low (<3%) contents of olivine and clinopyroxene. Groundmass textures are intergranular to intersertal.

The andesites are texturally homogeneous; they have porphyritic texture (P.I. about 14%) with plagioclase as the most abundant phenocrysts (10%), and low contents of augite (about 1%), ortho-pyroxenes (0.5%) and magnetite (0.6%). The groundmass texture is hyalopilitic with plagioclase, pyroxene and magnetite microcrystals set in fresh brown glass. Very rarely, a green amphibole is present as partially resorbed crystals. A strongly resorbed olivine crystal has been observed in one sample. Glomeroporphyritic clots made of plagioclase, pyroxenes, magnetite and entrapped glass are sometimes present. The mean of 3 point-counted modal analyses is reported in Table 2.

Mineral chemistry

Olivine

Olivine occurs as small (rarely exceeding 2 mm) euhedral phenocrysts and groundmass microphenocrysts in basalts and basaltic andesites. Some large (5-6 mm) rounded and embayed phenocrysts are present. Modal abundance does not exceed 5% (Table 2). Representative analyses are reported in Table 3 and plotted in Fig. 5. Olivine phenocrysts from basalts commonly present normal zoning (core-rim range Fo_{89}-Fo_{82}), but reverse zoning is also present. Groundmass microcrystals have the same composition of the rims. Crystals are always fresh; tiny Cr-spinel microcrystals are enclosed in phenocrysts. Olivine compositions change regularly from basalt to basaltic andesite (sample 1691), which has a Fo_{76} composition for phenocryst and Fo_{74} for groundmass. Olivine disappears with increasing silica content, and in andesites is replaced by orthopyroxene.

Table 3 — Representative point analyses of olivine.

	basalts					bas. and.		
	M1-1 c	M1-1 r	1663 c	1663 r	1663 mp	1691 c	1691 r	1691 mp
SiO_2	39.9	40.3	41.1	39.9	39.7	38.6	38.3	38.5
FeO	17.1	11.3	10.3	16.3	16.2	21.9	22.4	23.7
MnO	0.27	0.23	0.12	0.35	0.27	0.46	0.30	0.43
MgO	44.1	48.2	49.1	45.0	44.6	39.7	39.5	38.8
CaO	0.18	0.2	0.23	0.26	0.36	0.15	0.26	0.33
Total	101.55	100.23	100.85	101.81	101.13	100.81	100.8	101.76
Numbers of ions on the basis of 4 O								
Si	1.00	0.99	1.00	0.99	0.99	0.99	0.99	0.99
Fe	0.36	0.23	0.21	0.34	0.34	0.47	0.48	0.51
Mn	0.01	0.01	0.00	0.01	0.01	0.01	0.01	0.01
Mg	1.64	1.77	1.78	1.67	1.66	1.53	1.52	1.49
Ca	0.01	0.01	0.01	0.01	0.01	0.00	0.01	0.01
Total	3.01	3.01	3.00	3.01	3.01	3.01	3.01	3.01
X_{Mg}	.82	.88	.89	.83	.83	.76	.76	.74

c=core; r=rim; mp=groundmass microphenocryst.

The olivine-liquid equilibrium was evaluated by applying the Fe/Mg exchange coefficient (K_D=(FeO/MgO)ol (FeO/MgO)liq=0.33; Roeder and Emslie, 1970) to core composition and assuming a ratio Fe_2O_3/FeO of 0.20 for the whole-rock. The calculations suggest that olivine is in equilibrium with bulk rock, both in basalts and basaltic andesites.

Plagioclase

Selected analyses are reported in Table 4 and data points are plotted in Fig. 4.

In basalts, plagioclase phenocrysts are generally represented by clear and relatively unzoned crystals; crystals with dusty or cellular textures and glass inclusions are also present, but not abundant. Zoning patterns are generally normal but reverse zoning may be present. Core compositions are bimodal with one group clustered around An_{90} and another around An_{70} (see Fig. 4); rim compositions are scattered and display the same composition spread as the cores. Groundmass crystal compositions are scattered with a limited sodic enrichment with respect to the phenocrysts. The bimodal composition of the phenocryst cores could be an indication of two generations of phenocrysts.

The textures of andesite plagioclases are complex. Crystals with dusty or cellular textures and/or rich in glass inclusions are common. Zoning patterns are generally normal; compositional ranges from core to rim in phenocrysts and from phenocrysts to groundmass are wide. Sometimes phenocrysts with clear and unzoned cores overgrown by a rim of different composition (An_{41}) are present. These cores have a very high anorthite content (89-92) which is identical to that of cores of some basalt plagioclases. It is unlikely that these cores had crystallized from the andesitic magma because this would imply an unrealistically high water pressure ($P_{H2O} \geq$ 5Kb) (Gill, 1981). A possible explanation is that these cores actually represent xenocrysts inherited from basaltic magma.

Plagioclase textural and compositional complexity is typical of orogenic rocks and reflects a multi-stage history of crystallization and/or processes of magma mixing (Ewart, 1976, 1982; Gill, 1981; Sakuyama, 1981; Halsor and Rose, 1991).

Table 4 — Representative point analyses of plagioclases.

	basalts						bas. and.		
	M1-3 c	M1-3 r	M1-3 gms	M1-1 gms	1663 c	1663 r	1691 c	1691 r	1691 gms
SiO_2	45.6	48.5	48.2	50.1	51.6	48.3	46.2	52.9	51.9
Al_2O_3	34.5	31.4	31.8	30.7	30.7	32.3	35.1	29.7	30.5
FeO	0.41	0.84	0.91	0.67	0.24	0.51	0.58	0.95	1.00
CaO	18.4	15.4	15.6	14.5	13.8	15.9	18.1	12.8	13.7
Na_2O	0.91	2.3	2.2	3.2	3.5	1.9	1.0	3.9	3.1
K_2O	0.13	0.22	0.18	0.25	0.18	0.00	0.00	0.32	0.24
Total	99.95	98.66	98.89	99.42	100.02	98.91	100.98	100.57	100.44
Numbers of ions on the basis of 8 O									
Si	2.10	2.25	2.23	2.30	2.34	2.23	2.11	2.39	2.35
Al	1.88	1.72	1.74	1.66	1.64	1.76	1.89	1.58	1.63
Fe	0.02	0.03	0.04	0.03	0.01	0.02	0.02	0.04	0.04
Ca	0.91	0.77	0.77	0.71	0.67	0.79	0.88	0.62	0.66
Na	0.08	0.21	0.20	0.29	0.31	0.17	0.09	0.34	0.27
K	0.01	0.01	0.01	0.02	0.01	0.00	0.00	0.02	0.01
Total	5.00	4.99	4.99	5.00	4.99	4.97	4.98	4.98	4.96
X_{Ca}	.91	.78	.79	.70	.68	.82	.91	.63	.70
X_{Na}	.08	.21	.20	.28	.31	.18	.09	.35	.29
X_K	.01	.01	.01	.02	.01	.00	.00	.02	.01

	andesites								
	M2-3 c	M2-3 r	M2-1 c	M2-1 r	M2-1 gms	M2-2 c	M2-2 r	M2-2 gms	M2-2 gms
SiO_2	54.2	56.2	53.3	53.9	56.7	44.7	58.1	62.4	57.7
Al_2O_3	29.2	27.3	29.8	28.8	26.8	34.5	26.8	22.8	27.1
FeO	0.53	0.68	0.51	0.52	0.64	0.59	0.69	0.71	0.54
CaO	11.7	9.4	12.5	11.5	9.0	18.5	8.5	5.0	9.0
Na_2O	4.6	5.4	4.1	4.6	5.9	0.75	6.3	7.0	6.0
K_2O	0.25	0.38	0.26	0.27	0.56	0.00	0.55	1.80	0.51
Total	100.48	99.36	100.47	99.59	99.60	99.04	100.94	99.71	100.85
Numbers of ions on the basis of 8 O									
Si	2.44	2.54	2.40	2.45	2.56	2.08	2.58	2.78	2.57
Al	1.55	1.45	1.58	1.54	1.43	1.90	1.40	1.20	1.42
Fe	0.02	0.03	0.02	0.02	0.02	0.02	0.03	0.03	0.02
Ca	0.56	0.46	0.60	0.56	0.44	0.92	0.41	0.24	0.43
Na	0.40	0.47	0.36	0.41	0.52	0.07	0.54	0.61	0.52
K	0.01	0.02	0.02	0.02	0.03	0.00	0.03	0.10	0.03
Total	4.99	4.97	4.98	4.99	4.99	4.99	4.99	4.96	4.98
X_{Ca}	.58	.48	.62	.57	.44	.93	.41	.25	.44
X_{Na}	.41	.50	.37	.41	.53	.07	.56	.64	.53
X_K	.01	.02	.01	.02	.03	.00	.03	.11	.03

c = core, r = rim, gms = groundmass.

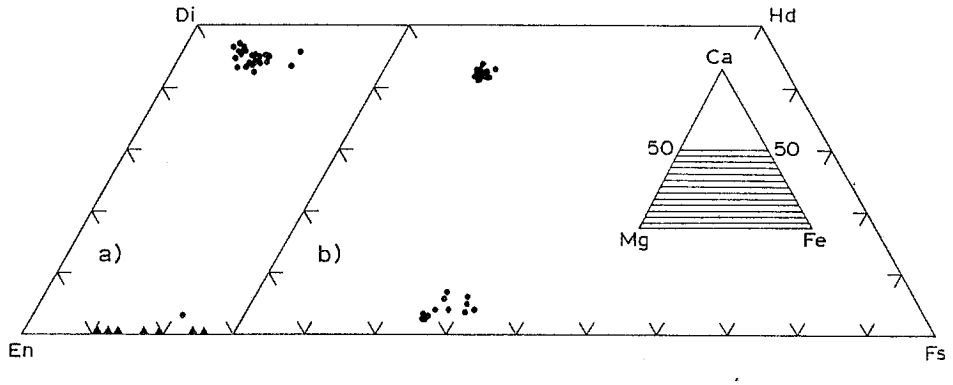

Fig. 5 — Calcium-Magnesium-Iron ternary diagram (section Diopside-Hedembergite-Enstatite-Ferrosilite) (Di-Hd-En-Fs) of pyroxenes in lavas from Marsili volcano; (a) = basalts, (b) = andesites. Olivine compositions plotted along the En-Fs join.

Table 5 — Representative point analyses of clinopyroxenes.

	basalts				bas. and.		andesites	
	M1-3 c	M1-3 r	M1-3 gms	M1-1 gms	1691 c	1691 r	M2-3 c	M2-3 r
SiO_2	51.1	51.5	45.9	49.3	52.0	49.7	51.9	51.3
TiO_2	0.40	0.16	1.55	1.11	0.39	0.66	0.47	0.61
Al_2O_3	4.2	3.5	8.4	5.9	3.3	4.5	2.3	2.9
Cr_2O_3	0.31	0.40	0.14	0.28	0.23	0.23	—	—
FeO	5.3	4.3	9.7	6.9	7.0	7.8	8.5	8.2
MnO	—	—	0.21	0.27	0.13	0.11	0.40	0.26
MgO	15.8	16.4	12.5	15.7	15.9	14.7	15.8	15.1
CaO	22.5	22.8	21.1	20.3	21.9	21.8	20.5	20.7
Na_2O	—	0.22	0.20	0.22	0.20	0.33	0.20	0.20
Total	99.61	99.28	99.70	99.98	101.05	99.83	100.07	99.27
Numbers of ions on the basis of 4 cations								
Si	1.88	1.89	1.72	1.81	1.89	1.84	1.92	1.91
Al^{iv}	0.12	0.11	0.28	0.19	0.11	0.16	0.08	0.09
Al^{vi}	0.06	0.04	0.09	0.07	0.04	0.03	0.02	0.04
Ti	0.01	—	0.04	0.03	0.01	0.02	0.01	0.02
Cr	0.01	0.01	—	0.01	0.01	0.01	—	—
Fe^{3+}	0.03	0.06	0.12	0.07	0.06	0.11	0.06	0.03
Fe^{2+}	0.14	0.07	0.18	0.14	0.15	0.13	0.21	0.23
Mn	—	—	0.01	0.01	—	—	0.01	0.01
Mg	0.87	0.90	0.70	0.86	0.86	0.81	0.87	0.84
Ca	0.89	0.90	0.85	0.80	0.85	0.86	0.81	0.83
Na	—	0.02	0.01	0.02	0.01	0.02	0.01	0.01
Wo	46.3	46.5	45.6	42.5	44.2	45.0	41.4	42.8
En	45.2	46.6	37.6	45.8	44.6	42.3	44.5	43.5
Fs	8.5	6.9	16.7	11.7	11.2	12.7	14.1	13.7
X_{Mg}	.84	.87	.70	.80	.80	.77	.76	.76

c = core, r = rim, gms = groundmass; $X_{Mg} = Mg/(Mg+\Sigma Fe)$.

Table 6 — Representative point analyses of orthopyroxenes.

	bas. and.	andesites				
	1691 r	M2-3 c	M2-3 r	M2-1 gms	M2-1 gms	M2-1 gms
SiO_2	55.2	53.8	53.0	52.6	50.6	53.3
TiO_2	—	0.14	0.20	0.22	0.78	0.25
Al_2O_3	1.6	1.3	1.6	1.5	2.2	1.7
FeO	14.0	16.1	16.0	17.9	19.0	16.5
MnO	0.31	0.76	0.66	0.94	0.75	0.71
MgO	28.9	26.7	25.9	22.5	23.6	25.4
CaO	1.7	1.5	1.3	3.1	1.8	2.1
Total	202.71	100.41	98.66	98.76	98.73	99.96
Numbers of ions on the basis of 4 cations per formula unit						
Si	1.94	1.94	1.95	1.96	1.88	1.94
Al^{iv}	0.06	0.06	0.06	0.04	0.10	0.06
Al^{vi}	—	—	0.01	0.03	—	0.01
Ti	—	—	0.01	0.01	0.02	0.01
Fe^{3+}	0.06	0.06	0.03	—	0.09	0.04
Fe^{2+}	0.35	0.43	0.46	0.56	0.50	0.47
Mn	0.01	0.02	0.02	0.03	0.02	0.02
Mg	1.51	1.43	1.42	1.25	1.31	1.38
Ca	0.06	0.06	0.05	0.12	0.07	0.08
Wo	3.2	2.9	2.6	6.3	3.6	4.1
En	75.8	71.7	71.6	63.7	65.6	69.4
Fs	21.0	25.4	25.9	30.0	30.8	26.4
X_{Mg}	.79	.74	.74	.69	.69	.73

c=core, r=rim, gms=groundmass; $X_{Mg}=Mg/(Mg+\Sigma Fe)$.

Pyroxenes

Clinopyroxenes

Augite phenocrysts are present in both basalts and andesites always with low modal abundances (<3%). Representative analyses are reported in Table 5, data points in Fig. 5. Basalt augites are relatively unzoned and cluster in a narrow area of the En-Fs-Wo diagram. The zoning patterns are both normal and reversed; the Fe-enrichment trend is very limited. Al_2O_3 and TiO_2 contents increase from core to rim and in groundmass crystals. Augites from andesites have an homogeneous composition and differ from basalt augites by being slightly more Fe-rich according to whole-rock composition. Mg/(Mg+Fe) ratios of clinopyroxene cores are similar to those of coexisting olivines. This is an indication of equilibrium between these two phases (Sakuyama, 1981).

Orthopyroxenes

Orthopyroxene appears in basaltic andesites as very scarce rims on augite phenocrysts, and in andesites as small (<1mm) phenocrysts and groundmass microcrystals. Modal abundance is always low (<1%). Selected analyses are reported in Table 6, data points in Fig. 5. In basaltic andesites, the scarce orthopyroxene has an En_{76} composition. In andesites, orthopyroxene phenocrysts are unzoned and have an En_{72} composition; groundmass microcrystals are of $En_{69\text{-}64}$ composition. The appearance of orthopyroxene is related to the silica content of the magma. The mineral appears in basaltic andesites in very small quantities and coexists with olivine; its abundance increases in andesites where olivine disappears completely.

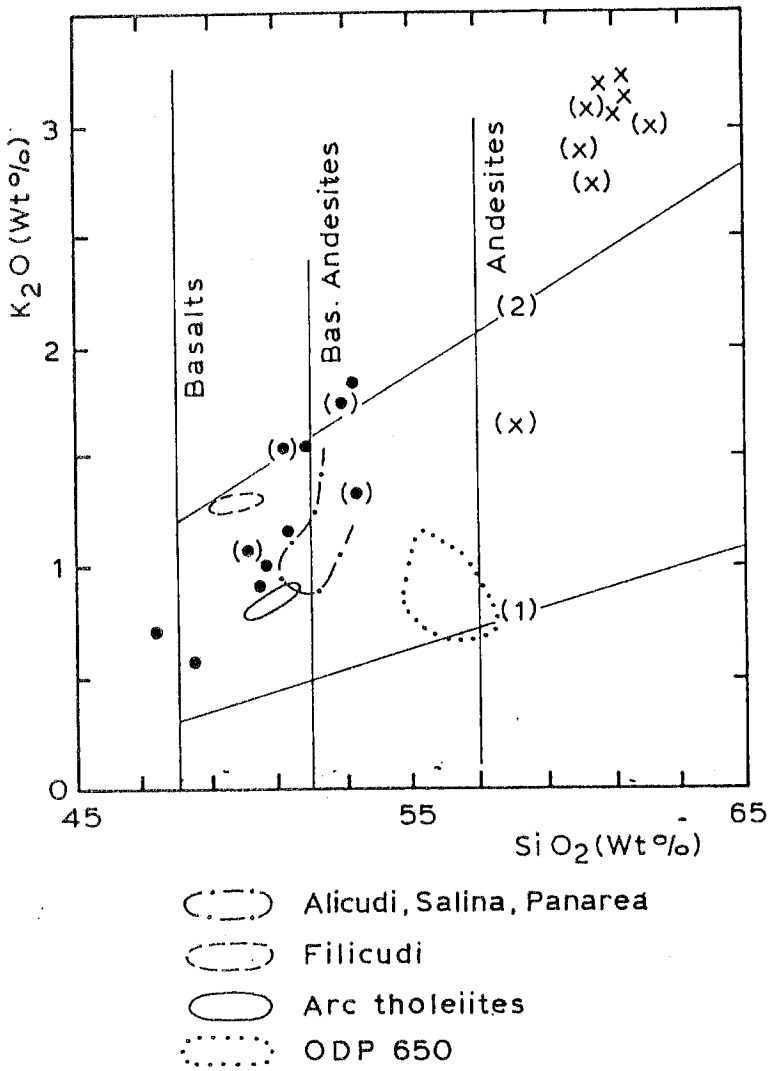

Fig. 6 — K_2O vs SiO_2 relationship for the Marsili volcanics. Filled circles = basalts and andesitic basalts, crosses = andesites, brackets = data from Maccarrone (1970), Keller and Leiber (1974) and Selli et al. (1977). Boundary lines of different associations according to Le Maitre (1989): (1) = low-K to medium-K, (2) = medium-K to high-K.

Oxides

Selected compositions are reported in Table 7. In basalts, oxides are almost completely absent, being represented only by very small groundmass crystals and very small Cr-Al spinel crystals enclosed in olivine phenocrysts. Titanomagnetite appears as scarce microphenocrysts in basaltic andesites and as well-developed microphenocrysts (0.3-0.5 mm) in andesites (modal abundance about 0.5 - 1%). The appearance of magnetite may be related to an increasing magma water content, since water disassociation will increase oxygen fugacity (fO_2) favouring magnetite crystallization (Halsor and Rose, 1991).

Amphibole

One partially resorbed green amphibole crystal has been observed in one andesite sample.

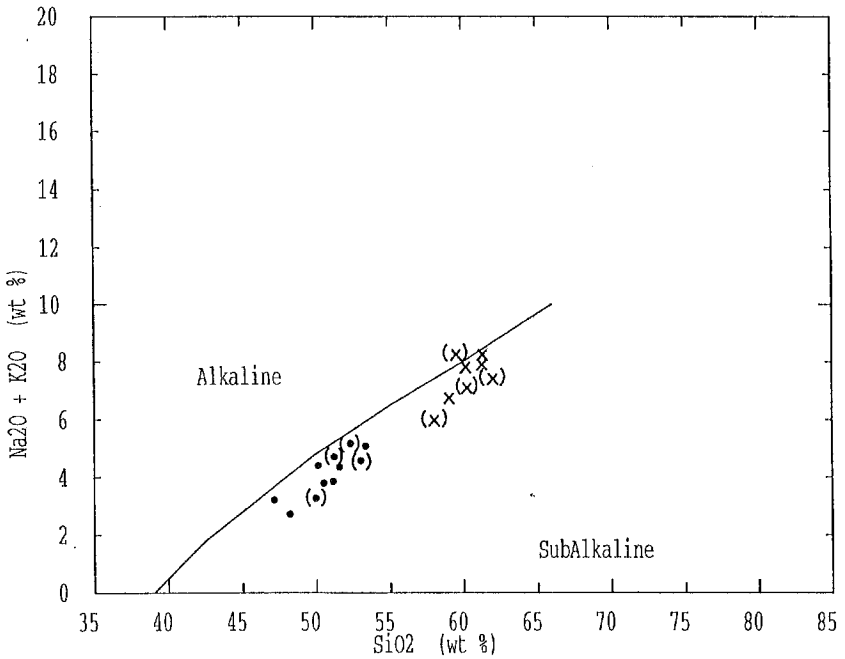

Fig. 7 — Alkalies vs SiO_2 plot of lavas from Marsili volcano. The dividing line is after Irvine and Baragar (1971). Dotted line indicates the andesites field from ODP Hole 650.

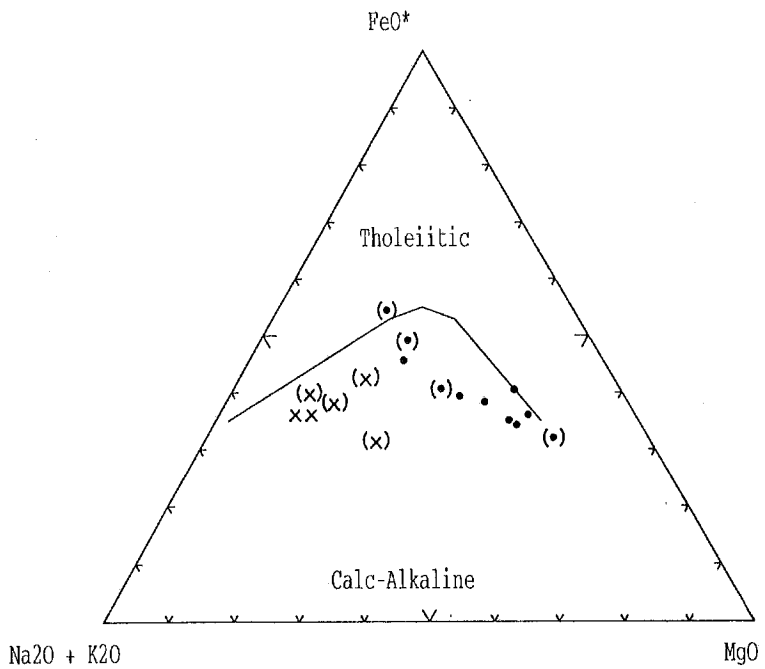

Fig. 8 — Ternary diagram Alkalies-MgO-FeO* of lavas from Marsili volcano. The dividing line between CA and THO fields after Irvine and Baragar (1971). Dotted line indicates the andesites field from ODP Hole 650.

Table 7 — Representative point analyses of spinels.

	basalts		bas. and.	and.
	M1-1	1663	1691	And
SiO_2	—	—	0.25	0.20
TiO_2	0.47	0.52	9.7	13.2
Al_2O_3	22.2	30.8	5.8	3.4
Cr_2O_3	40.7	28.8	—	—
FeO	21.6	24.7	3.4	74.1
MnO	0.08	0.11	0.35	0.70
MgO	14.8	14.4	5.8	3.3
Total	99.85	99.33	5.30	94.90
Fe_2O_3*	9.16	10.54	5.93	40.06
FeO*	13.36	15.20	2.07	38.06
Total	100.77	100.37	99.90	98.92
Numbers of ions on the basis of 3 cations				
Si	—	—	0.01	0.01
Al	0.79	1.07	0.24	0.15
Ti	0.01	0.01	0.26	0.37
Cr	0.98	0.67	—	—
Fe^{3+}	0.21	0.23	1.22	1.11
Fe^{2+}	0.34	0.38	0.95	1.17
Mn	—	—	0.01	0.02
Mg	0.67	0.63	0.31	0.18

Fe_2O_3*, FeO* recalculated from stoichiometry. And = mean of 12 magnetite analyses from andesites.

The appearance of this mineral is interesting because it suggests the presence of a water-rich magma.

Chemistry

Major and trace element analyses of four selected samples are reported in Table 8.

Fig. 6 shows the K_2O versus SiO_2 contents of calc-alkaline volcanic rocks from 20 sampling stations distributed over a large depth interval of the Marsili seamount (Fig. 3). Only at one dredging site, CT69/27 (Table 1; Selli et al.,1977), were recovered basalts whose petrochemical characteristics indicate an affinity with oceanic island basic products. These rocks will not be treated here. The plotted samples are represented by basalts, basaltic andesites (in minor amount) and andesites of calc-alkaline and high-K calc-alkaline affinity. In the Fig. 6, the composition fields of basaltic rocks of calcalkaline serial affinity, that is of 'normal' K contents, from the Aeolian arc (Keller, 1974a; Villari, 1980a, b and c), and the basaltic andesite field from the deep igneous crust of Marsili basin (ODP site 650; Beccaluva et al., 1990) are also plotted. The Alicudi, Salina and Panarea rocks include also terms with the silica-poor CA basaltic andesite composition.

The diagrams Alkalies-SiO_2 of Fig. 7, and Alkalies-FeO*-MgO of Fig. 8 (Irvine and Baragar, 1971) indicate that the studied samples are subalkaline in character and belong to subduction related volcanic associations of the plate convergence zones.

The Fig. 3 shows that basalts and andesitic basalts occur in the low to intermediate areas of Marsili, while the andesites are present mainly at the summit of the edifice.

The histogram of Fig. 9 shows the bimodal nature of the Marsili volcanites, whose frequency minimum corresponds to the silica range of basaltic andesites (52 to 56% of SiO_2).

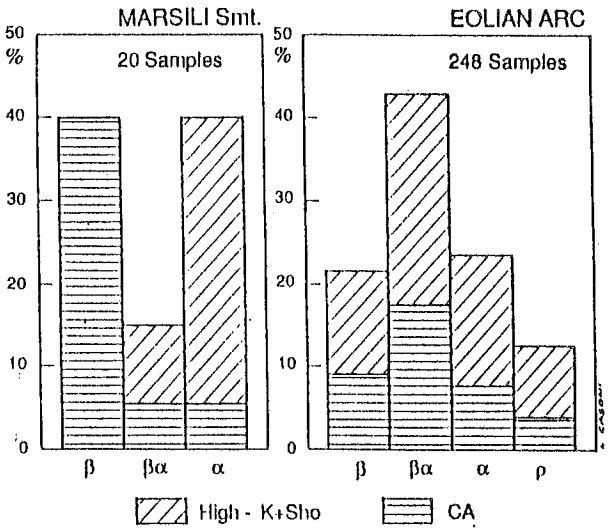

Fig. 9 — Frequency histograms of the Marsili and Aeolian arc volcanics divided, on the basis of SiO_2 contents, into basalt (beta), basaltic andesite (beta/alpha), andesite (alpha), rhyolite (rho) rock types and on the basis of K_2O contents into CA, and high-K to shoshonitic, serial affinities.

Table 8 — Selected rock analyses.

	M1-3	M1-1	1691	M2-1
SiO_2	47.15	49.40	52.40	60.10
TiO_2	0.61	0.78	1.00	0.96
Al_2O_3	18.60	16.53	18.06	16.70
Fe_2O_3	7.49	7.51	9.00	6.12
MnO	0.12	0.12	0.14	0.13
MgO	7.04	9.14	4.02	1.97
CaO	13.98	10.64	9.03	4.35
Na_2O	2.12	2.74	3.30	4.87
K_2O	0.56	1.00	1.79	3.11
P_2O_5	0.25	0.34	0.40	0.44
LOI	1.84	1.53	0.59	0.90
Total	99.76	99.73	99.73	99.65
Rb	13	22	52	87
Sr	597	397	558	374
Y	16	21	26	35
Zr	53	71	101	197
Nb	6	9	14	25
Ba	207	494	569	1175
Ni	77	163	25	13
Cr	129	328	14	5
V	172	198	249	1124
X_{Mg}	.69	.74	.51	.43

X_{Mg}=Mg/(Mg+Fe); Fe_2O_3/FeO=0.2.

DISCUSSION

Mineralogy

From the point of view of mineral chemistry, the analyzed rocks from Marsili show the typical features of orogenic rocks (Ewart, 1976; 1982). The following characteristics are present, and are mainly indicative of fractional crystallization processes (Halsor and Rose, 1991; Koyaguchi, 1986; Sakuyama, 1981):

1) The Mg-Fe exchange coefficient between olivine and liquid in the samples suggests that olivine is in equilibrium with host-rocks. 2) Mg#'s of olivine and augite are similar (Tables 3 and 5) and decrease regularly with increasing bulk-rock FeO*/MgO ratios. 3) The En-Fs-Wo triangle shows an iron enrichment trend for pyroxenes. 4) Phenocryst assemblages change regularly with increasing SiO_2; olivine, present in basalts, is associated with orthopyroxene in basaltic andesites and disappears in the more silica-rich andesites; plagioclase in andesites are more sodic than in basalts; clinopyroxene is more Fe-rich in andesites. 5) Plagioclase phenocrysts are normally zoned; groundmass microphenocryst are more sodic than phenocrysts. The occurrence in andesites of some plagioclase phenocrysts with very anorthite-rich (91%) cores, identical to the composition of cores of basalt plagioclases, could be an indication that some andesite plagioclase cores actually represent relict minerals inherited from basalts (xenocrysts?). This plagioclase mineralogy may be an evidence for magma mixing. Plagioclases show some disequilibrium features, but overall their compositions are correlated with bulk-rock. 6) The fact that oxides are absent in basalts, very scarce in basaltic andesites, and abundant in andesites is an indication of increasing oxygen fugacity. This may be explained by an increase in water pressure. Precipitation of an anhydrous mineral assemblage, such as that of the basalts (olivine, plagioclase, clinopyroxene), could increase the water content of the fractionated liquids.

The presence of mineralogical features very similar to those mentioned above in the orogenic rock suite from Lipari (Aeolian Islands) was considered (Bargossi et al., 1989) to represent the expression of a magmatic evolution governed by fractional crystallization.

Chemistry

In contrast to previous ideas, derived mainly from structural features (C.N.R., 1981), which attributed an ocean-island basalt (OIB) nature to the basal lavas of Marsili seamount, the more extensive sampling now available shows that the volcano consists of products of calcalkaline, subduction related nature. The only exception to this are the rocks of OIB affinity sampled at one dredge site (Selli et al., 1977). The petrochemical characteristics of Marsili are, thus, unlike those of the large central volcanoes of the Tyrrhenian, Vavilov and Magnaghi, whose lava samples indicate an affinity with the OI basalts (Selli et al., 1977; Robin et al., 1987).

The orogenic magmatism of Marsili volcano is characterized by a transition from calc-alkaline basalts to andesites of high-potassium (HK-CA) serial character which constitute the top of the seamount. Also in the volcanic edifices of the Aeolian arc (Keller, 1974a; Villari, 1980a, b and c; Beccaluva et al., 1985), and in the volcanoclastic sediments of the ODP Site 650 (McCoy and Cornell, 1990; Calanchi et al., 1994) the stratigraphically higher volcanites are more enriched in K compared to the underlying ones.

The calcalkaline subduction-related volcanites of the Aeolian arc have ages from about 1 Ma to the Present and notably diverse chemical compositions ranging from the arc-tholeiites of North Lametini seamount to the leucite-tephrites of the islands of Stromboli and Vulcano. The patterns of the histogram of Fig. 9, although possibly biased by the sampling, in particular in the submarine areas, suggest that the distribution of magmatic types represents a distinguishing feature between the Marsili back-arc and the Aeolian arc volcanic edifices. It can be seen that there is a continuum basalt - basaltic andesite - andesite of the products from the Aeolian arc. In contrast to the Marsili seamount, the most abundant rock type of the Aeolian volcanism are basaltic andesites.

The nature and location of the Marsili magmatism suggest the absence, in the south Tyrrhenian volcanic area, of an overall spatial relationship of K_2O contents with depth to the underlying Benioff structure. In fact, if this were the case, the volcanites of Marsili, being emplaced above

a deeper part of the Benioff zone, would be richer in potassium than those of the Aeolian arc at equivalent SiO_2 values.

A temporal relationship characterizes the single volcanic centers of the south Tyrrhenian, since overall, as in other orogenic regions (Morrison, 1980), K-enriched lavas occupy higher positions in the stratigraphical sequences.

It should be noted that, on the basis of the mineral chemistry data, fractional crystallization could contribute significantly to the origin of the observed rock suite of the Marsili magmatism, from basalt to basaltic andesite to andesite. However, it has been recognized that the transitions from calc-alkaline to more K-rich manifestations (s.l.) of the Aeolian arc volcanoes can be (Barberi et al., 1974; Keller, 1974a; Villari, 1980c) a response to rapid foundering of the Benioff structure of the south Tyrrhenian. According to this interpretation, generation of high-potassium andesite magma in the late stage of the Marsili volcanism, subsequent to the effusion of early basalt lavas, could reflect detachment and sinking of the subducted lithosphere into the underlying mantle.

Tectonism and geodynamic considerations

The Marsili area (seamount and deep basin) was affected by tectono-magmatic faults related to rifting and spreading. The extensional linear faults of Marsili volcano were, initially, N-S to NNE-SSW trending (Selli et al., 1977; Sborshchikov et al., 1988 and 1990). The subsequent, NE-SW direction of the spreading mechanisms in the top of Marsili resulted from a clockwise rotation of about 20° (Fig. 1) of the early fissural trends. This variation of extension direction could correlate with the change of magma composition from calc-alkaline basalts to HK-CA andesites of the edifice top.

A roll-back of the Tyrrhenian subduction hinge zone and migration of the arc volcanism (Savelli 1988; Francalanci and Manetti, this vol.) took place from the island of Sardinia (32-13 Ma), to the central Tyrrhenian Sea (4-2 Ma?), to the Aeolian area (1-0 Ma). The NW-SE trending, conjugate faulting related to the late NW-SE extension of Marsili seamount may belong to the magmato-tectonic alignment of Taormina-Lipari which has the same orientation (Fig. 1). The alignment seems to be located at the western edge of the area of Tyrrhenian deep seismicity (Fig. 2). This first order lineation zone of right-lateral strike-slip movements extending from Taormina to the islands of Lipari-Salina-Vulcano, in the central part of the Aeolian arc, and to the top of Marsili is affected by a recent volcanic-tectonic activity. In particular, shallow depth seismicity is intense in the active arc sector of the tectonic lineation (Neri et al., 1991) and NW-SE and NE-SW oriented fault systems characterize the evolution of the central Aeolian islands (e.g., Gabbianelli et al., 1990).

Important E-W trending tectonic lineation zones of strike-slip displacement (Boccaletti et al., 1984, 1990; Finetti and Del Ben, 1986; Lavecchia, 1988; Savelli and Schreider, 1991; Locardi and Nicolich, 1992) border the Marsili deep basin to the north and south. These are known, respectively, as the Palinuro volcano and the Sicilian slope fault zones.

The distribution of deep seismic events (Fig. 2) indicates a regime of convergence characterized by the presence of subducting lithosphere which is oblique to the arc (Barberi et al., 1974; Morrison, 1980; Giardini and Velona', 1991). The post-collisional volcanism, the dismembering and displacement to greater depth of the subducted lithosphere occur in the presence of intense subsidence and rifting of the seamount and basin of Marsili (Finetti and Del Ben, 1986; Kastens et al., 1986; 1988; Mascle and Rehault, 1990; Sborshchikov et al., 1990). This tectonic setting is in agreement with the suggestion of Gasparini et al. (1982) and Giardini and Velona' (1991) that the south Tyrrhenian Benioff zone is in an advanced, senile stage of its evolution.

The axial fractures feeding the seamount volcanism are located (Fig. 2) between the deep seismogenic area with the highest energy release, to the east, and that, to the west, which has the deepest but less numerous seismic events. Therefore, the Marsili volcanic edifice lies in proximity to the observed gap of the deep seismicity - maybe, a zone of high attenuation of the seismic waves - and to the change of dip to the Benioff zone. Active subduction processes may have ceased. At the Present is hypothesized the existence of a passive subduction of the

residual slab, subsequen to its fragmentation in the asthenosphere. Igneous crust generation and lithosphere evolution in the south Tyrrhenian volcanic area were accompanied (Sartori, 1990; Doglioni, 1991) by overthrusts and drifting of the adjoining, more external sectors of the Africa-Adria-verging orogenic systems (south Apennines-Calabrian arc, Sicilian Maghrebids).

Acknowledgements. The studied lava samples from Marsili seamount were recovered during two cruises of the R/V Vityaz (1986) and Akademic Mstislav Keldysh (1988) of the Institute of Oceanology of the Russian Academy of Sciences to which participated one of us (CS). V.S. Yastrebov, A.A. Schreider, I.M. Sborshchikov and E.M. Emelyanov are thanked for stimulating discussions and G. Simboli and N. Calanchi for critical reading of the manuscript. This work was supported by a MUR 60% contribution (G. Simboli). This is IGM-CNR contribution N. 871.

REFERENCES

Anderson H. and Jackson J.; 1987: *The deep seismicity of the Tyrrhenian Sea.* Geophys. J. R. Astron. Soc., **91**, 613-637.

Barberi F., Innocenti F., Ferrara G., Keller J. and Villari L.; 1974: *Evolution of Eolian arc volcanism (Southern Tyrrhenian Sea).* Earth Planet. Sci. Lett., **21**, 269-276.

Bargossi G. M., Campos Venuti M., Gasparotto G. e Rossi P. L.; 1989: *Petrologia e stratigrafia delle successioni andesitiche l.s. di Lipari, Isole Eolie, Italia.* Miner. Petrogr. Acta, **32**, 295-326.

Beccaluva L., Gabbianelli G., Lucchini F., Rossi P. L. and Savelli C.; 1985: *Petrology and K/Ar ages of volcanics dredged from the Eolian seamounts: implications for the geodynamic evolution of the Southern Tyrrhenian basin.* Earth Planet. Sci. Lett., **74**, 187-208.

Beccaluva L., Bonatti E., Dupuy C., Ferrara G., Innocenti F., Lucchini F., Macera P., Petrini R., Rossi P. L., Serri G., Seyler M. and Siena F.; 1990: *Geochemistry and mineralogy of volcanic rocks from ODP Sites 650, 651, 655 and 654 in the Tyrrhenian Sea.* In: Proceedings of the Ocean Drilling Program, Scientific Results, Vol. 107, pp. 49-74.

Boccaletti M., Nicolich R. and Tortorici L.; 1984: *The Calabrian arc and the Ionian sea in the dynamic evolution of the Central Mediterranean.* Marine Geology, **55**, 219-245.

Boccaletti M., Nicolich R. and Tortorici L.; 1990: *New data and hypothesis on the development of the Tyrrhenian basin.* Palaeo- geology, -climatology, -ecology, **77**, 15-40.

Calanchi N., Gasparotto G. and Romagnoli C.; 1994: *Glass chemistry in volcaniclastic sediments of site 650, Leg 107 sedimentary sequence: Provenance and chronological implications.* J. of Volcanol and Geoth. Res., in press.

C.N.R.; 1981: *Carta tettonica d'Italia. Scala 1:1500000.* CNR, Prog. Final. Geodinamica, Pubbl., N. 269. Graf. Edit. Cart. Spa Roma.

Crisci G. M., De Rosa R., Esperanza S., Mazzuoli R. and Sonnino M.; 1991: *Temporal evolution of a three component system: the island of Lipari (Aeolian Arc, southern Italy).* Bull. Volcanol., **53**, 207-221.

Doglioni C.; 1991: *A proposal of kinematic modeling for W-dipping subductions - Possible applications to the Tyrrhenian-Apennines system.* Terra Nova, **3**, 423-434.

Doglioni C.; 1992: *Main differences between thrust belts.* Terra Nova, **4**, 152-164.

Ewart A.; 1976: *Mineralogy and chemistry of modern orogenic lavas - some statistics and implications.* Earth Planet. Sci. Lett., **31**, 417-432.

Ewart A.; 1982: *The mineralogy and petrology of Tertiary-Recent orogenic volcanic rocks: with special reference to the andesitic-basaltic compositional range.* In: Thorpe R.S. (ed) 'Andesites', John Wiley & Sons, New York.

Finetti I. and Del Ben A.; 1986: *Geophysical study of the Tyrrhenian opening.* Boll. Geof. Teor. Appl., **28**, 75-155.

Francalanci L., Manetti P. and A. Peccerillo; 1989: *Volcanological and magmatological evolution of Stromboli volcano (Aeolian Islands): the roles of fractional crystallization, magma mixing, crustal contamination and source heterogeneity.* Bull. Volcan., **51**, 355-378.

Francalanci L., and Manetti P.; 1994: *Geodynamic models of the southern Tyrrhenian region: constraints from petrology and geochemistry of the Aeolian volcanic rocks.* Boll. Geof. Teor. Appl., **36**, 00-00.

Gabbianelli G., Gillot P.Y., Lanzafame G., Romagnoli C. and Rossi P.L.; 1990: *Tectonic and volcanic evolution of Panarea (Aeolian Islands, Italy).* Marine Geol., **92**, 313-326.

Gasparini C., Iannaccone G., Scandone P. and Scarpa R.; 1982: *Seismotectonics of the Calabrian arc.* Tectonophys., **84**, 267-286.

Gasperini M.; 1993: *Global forces on the lithosphere.* J. of Geodynamics, **17/3**, 121-132.

Giardini D. and Velona' M.; 1991: *The deep seismicity of the Tyrrhenian Sea.* Terra Nova, **3**, 57-64.

Gill J. B.; 1981: *Orogenic andesites and plate tectonics.* Springer Verlag, 358 pp.

Govindaraju K. and Mevelle G.; 1987: *Fully automated dissolution and separation methods for inductively coupled plasma atomic emission spectrometry rock analysis. Application to the determination of Rare Earth Elements.* J. of Analytic Atomic Spectrometry, **2**, 615-621.

Halsor S. P. and Rose W. I.; 1991: *Mineralogical relations and magma mixing in calk-alkaline andesites from Lake Atitlan, Guatemala.* Mineralogy and Petrology **45**, 47-67.

Irvine T. N. and Baragar W. R. A.; 1971: *A guide to the chemical classification of the common volcanic rocks.* Canad. J. Earth Sci., **8**, 523-548.

Jarosewich E., Nelen J. A. and Norberg J. A.; 1980: *Reference samples for Electron Microprobe Analysis.* Geostandars Newsletters, **4**, 43-47.

Kastens K., Mascle J., Auroux C., Bonatti E., Broglia C., Channell J.E.T, Curzi P., Emeis K.C., Glacon G., Hasegawa S., Hieke W., Mascle G., McCoy F., McKenzie J., Mascle G., Mendelson J., Mueller C., Rehault J-P., Robertson A., Sartori R., Sprovieri R. and Torii M.; 1986 *Young Tyrrhenian Sea evolved very quickly.* Geotimes, **31**, 11-14.

Kastens K., Mascle J., Auroux C. & Coll., ODP Leg 107 Scientific Party; 1988: *ODP Leg 107 in the Tyrrhenian sea: Insights into passive margin and back-arc basin evolution.* Geol. Soc. Amer. Bull., **100**, 1140-1156.

Keller J. and Leiber J.; 1974: *Sedimente, Tephra-lagen und Basalte der sudtyrrhenischen Tiefsee-ebene im Bereich des Marsili Seeberges.* Meteor. Forsch. Ergebn., Reihe C, N. **19**, 62-76.

Keller J.; 1974a: *Petrology of some volcanic rock series of the Aeolian arc, southern Tyrrhenian sea: calc-alkaline and shoshonitic associations.* Contrib. Mineral. Petrol., **46**, 29-47.

Koyaguchi T.; 1986: *Textural and compositional evidence for magma mixing and its mechanism, Abu volcano group, Southwestern Japan.* Contrib. Mineral. Petrol., **93**, 33-45.

Lavecchia G.; 1988: *The Tyrrhenian-Apennines system: structural setting and seismotectogenesis.* Tectonophys., **147**, 263-296.

Le Maitre R.W.; 1989: *A classification of igneous rocks and glossary of terms.* Blackwell, Oxford, 193 pp.

Locardi e Nicolich R.; 1992: *Geodinamica del Tirreno e dell'Appennino centro-meridionale: la nuova carta della Moho.* Mem. Soc. Geol. It., **41**, 121-140.

Maccarrone E.; 1970: *Notizie petrografiche e petrochimiche sulle lave sottomarine del seamount 4 (Tirreno sud).* Boll. Soc. Geol. Ital., **89**, 159-180.

McCoy F.W. Cornell W.; 1990: *Volcaniclastic sediments in the Tyrrhenian basin.* Proceedings of the Ocean Drilling Program, **107**, 291-306.

Mascle J. and Rehault J.P.; 1990: *A revised seismic stratigraphy of the Tyrrhenian Sea: implications for the basin evolution.* Proceedings of the ODP, Scient. Results, **107**, 617-636.

Morelli C., Giese P., Cassinis R., Colombi B., Guerra I., Luongo G., Scarascia S. and Schutte K.G.; 1975: *Crustal structure of Southern Italy. A seismic refraction profile between Puglia, Calabria, Sicily.* Boll. Geofis. Teor. Appl., **17**, 183-210.

Morrison G.W.; 1980: *Characteristics and tectonic setting of the shoshonite rock association.* Lithos, **13**, 97-108.

Neri G., Caccamo D., Cocina O. and Montalto A.; 1991: *Shallow earthquake features in the southern Tyrrhenian region: geostructural and tectonic implications.* Boll. Geof. Teor. Appl., **33**, 47-60.

Nicolich R.; 1981: *Crustal structures in the Italian Peninsula and surrounding seas: a review of DSS data.* In Wezel F.C. (ed), Sedimentary basins of Mediterranean margins, Tecnoprint, Bologna, pp. 3-17.

Peccerillo A. and Wu T.W.; 1992: *Evolution of calc-alkaline magmas in continental arc volcanoes: Evidence from Alicudi, Aeolian arc (Southern Tyrrhenian Sea, Italy).* J. Petrol., **33**, 1295-1315.

Puchelt H., Laschek D., et alii; 1986: *Forschungsfahrt Sonne 41, HYMAS 1. Fahrtbericht.* Institut f. Geochemie, Univ. Karlsruhe, 331 S. (pp.).

Ritsema A.R.; 1979: *Active or passive subduction at the Calabrian arc.* Geologie Mijnb., **58**, 127-134.

Robin C., Gennesseaux M., Colantoni P. and Vanney J.R.; 1987: *Vavilov seamount: a mild alkaline Quaternary volcano in the Tyrrhenian basin.* Mar. Geol., **78**, 125-136.

Roeder R. L. and Emslie R. F.; 1970: *Olivine-liquid equilibrium.* Contrib. Mineral. Petrol. **29**, 275-289.

Sakuyama M.; 1981: *Petrological study of the Myoko and Kurohine volcanoes, Japan: crystallization sequence and evidence for magma mixing.* Journal of Petrology, **22**, 553-583.

Sartori R.; 1990: *Evoluzione neogenico-recente del bacino tirrenico e suoi rapporti con la geologia delle aree circostanti.* Giorn. Geol., **51**, 1-39.

Savelli C.; 1988: *Late Oligocene to Recent episodes of magmatism in and around the Tyrrhenian Sea: Implications for the processes of opening in a young inter-arc basin of intra-arc-orogenic (Mediterranean) type.* In: Wezel F.C. (ed), The origin of arcs. Tectonophysics, **146**, 163-181.

Savelli C.; 1993: *Il rifting del vulcano Marsili (Mar Tirreno): aspetti morfotettonici osservati da bordo del sottomarino MIR 2.* Giorn. Geol., **54**, 215-227.

Savelli C. and Gasparotto G.; 1994: *Calcalkaline magmatism and rifting of Marsili deep-water volcano (Aeolian back-arc. southeastern Tyrrhenian sea).* Mar. Geol., in print.

Savelli C. and Schreider A. A.; 1991: *The opening processes in the deep Tyrrhenian basins of Marsili and Vavilov, as deduced from magnetic and chronological evidence of their igneous crust.* In: Francheteau J., Eldholm O. and Miles P. (eds), The Geology, Geophysics and Metallogeny of the Present-Day Oceans. Tectonophys., **190**, 119-131.

Sborscchikov I. M., Savelli C., Puchelt, H., Pescatore T., Schreider, A.A. and Yastrebov V.S.; 1988: *Some volcano-tectonic features of Marsili seamount (Tyrrhenian Sea): First report of two submersible dives.* In: Meeting of the Ital. Miner. and Petrol. Soc., Collected abstracts, Trieste, 8-9 December 1988, pp. 60-61.

Sborshchikov I. M., Savelli C. and Dukov N.; 1990: *Detailed side-sonar survey of summit of Marsili volcano: rifting morphology of an active axial zone of Tyrrhenian sea.* Giorn. Geol., **51**, 109-116.

Scandone P.; 1980: *Origin of Tyrrhenian Sea and Calabrian arc.* Boll. Soc. Geol. It., **98**, 27-34.

Selli R., Lucchini F., Rossi P.L., Savelli C. e Del Monte M.; 1977: *Dati geologici, petrochimici e radiometrici sui vulcani centro-tirrenici.* Giorn. Geol., **42**, 221-246.

Villari L.; 1980a. *The Island of Alicudi.* Rend. Soc. Ital. Miner. Petrol., **36**, 441 - 466.

Villari L.; 1980b. *The Island of Filicudi.* Rend. Soc. Ital. Miner. Petrol., **36**, 467 - 488.

Villari L.; 1980c. Ed.; *The Aeolian islands: an active arc in the Mediterranea sea.* Rend. Soc. Ital. Miner. Petrol., **36**, 335-533.

Wang C., Kastens K. and Hwang W.; 1991: *Rapid subsidence of small oceanic basins: a study of the Marsili Basin, Central Mediterranean.* J. Geophys. Res., 96-B3, 4413-4421.